NeuroImage 231 (2021) 117853

Contents lists available at ScienceDirect

NeuroImage

journal homepage: www.elsevier.com/locate/neuroimage

Behavioral validation of novel high resolution attention decoding method from multi-units & local field potentials

Carine De Sousa[1,*], C. Gaillard[1], F. Di Bello, S. Ben Hadj Hassen, S. Ben Hamed[*]

Institut des Sciences Cognitives Marc Jeannerod, CNRS UMR 5229, Université Claude Bernard Lyon I, 67 Boulevard Pinel, 69675 Bron Cedex, France

ARTICLE INFO

Keywords:
Monkey
Prefrontal cortex
Attention
LFP
Machine learning
Decoding

ABSTRACT

The ability to access brain information in real-time is crucial both for a better understanding of cognitive functions and for the development of therapeutic applications based on brain-machine interfaces. Great success has been achieved in the field of neural motor prosthesis. Progress is still needed in the real-time decoding of higher-order cognitive processes such as covert attention. Recently, we showed that we can track the location of the attentional spotlight using classification methods applied to prefrontal multi-unit activity (MUA) in the non-human primates. Importantly, we demonstrated that the decoded (x,y) attentional spotlight parametrically correlates with the behavior of the monkeys thus validating our decoding of attention. We also demonstrate that this spotlight is extremely dynamic. Here, in order to get closer to non-invasive decoding applications, we extend our previous work to local field potential signals (LFP). Specifically, we achieve, for the first time, high decoding accuracy of the (x,y) location of the attentional spotlight from prefrontal LFP signals, to a degree comparable to that achieved from MUA signals, and we show that this LFP content is predictive of behavior. This LFP attention-related information is maximal in the gamma band (30–250 Hz), peaking between 60 to 120 Hz. In addition, we introduce a novel two-step decoding procedure based on the labelling of maximally attention-informative trials during the decoding procedure. This procedure strongly improves the correlation between our real-time MUA and LFP based decoding and behavioral performance, thus further refining the functional relevance of this real-time decoding of the (x,y) locus of attention. This improvement is more marked for LFP signals than for MUA signals. Overall, this study demonstrates that the attentional spotlight can be accessed from LFP frequency content, in real-time, and can be used to drive high-information content cognitive brain-machine interfaces for the development of new therapeutic strategies.

1. Introduction

Accessing cognitive functions in real time, using machine learning methods applied to ongoing brain signals is considered as one of the major challenges of modern neurosciences, in order to enhance and restore human brain capacities (Astrand et al., 2014b; Cinel et al., 2019; Dresler et al., 2018). Indeed, the ability to decode brain information in real-time is expected to allow for a better characterization of cognitive functions and development of therapeutic applications based on brain-machine interfaces. While great success has been achieved in the field of neural motor prosthesis (Prochazka, 2017), real-time decoding of higher-order cognitive processes such as spatial attention is still hampered by the complexity of these mechanisms. One major issue in this respect is the fact that cognitive functions are mostly covert and can only be inferred transiently through subjects' behaviors. Another crucial issue is the fact that cognitive processes are highly dynamic, irrespectively of behavioral goals or instructions (Gaillard et al., 2020).

In the last years, we have recorded multi-unit activity (MUA) signals from prefrontal frontal eye fields (FEF), a cortical region at the core of attention selection (Buschman and Miller, 2007; Ekstrom et al., 2008; Gregoriou et al., 2009; Ibos et al., 2013; Moore and Fallah, 2001; Wardak et al., 2006). We report real-time access to the (x,y) coordinates of attentional spotlight from these ongoing prefrontal neuronal population spiking activity, at high spatial and temporal resolution (Astrand et al., 2020; Di Bello et al., 2020; Gaillard et al., 2020). Importantly, we show a strong correlation between the decoded (x,y) attentional spotlight in real-time and subjects' behavioral performance on a complex perceptual task.

In the following, we extend this (x,y) decoding of the attentional spotlight to local field potential (LFPs) signals, moving a step closer to real-time EEG based decoding of the attentional function. Indeed, LFP signals reflect the spiking activity that are summed over a large pop-

* Corresponding authors.
E-mail addresses: carine.desousa@isc.cnrs.fr (C. De Sousa), benhamed@isc.cnrs.fr (S. Ben Hamed).
[1] These two authors contributed equally to this work

https://doi.org/10.1016/j.neuroimage.2021.117853
Received 9 September 2020; Received in revised form 3 February 2021; Accepted 4 February 2021
Available online 11 February 2021

ulation of neurons while MUA refers to the activity of individual neurons or of a local population of neurons. While MUA activity is often best analyzed in the time-amplitude domain, LFPs are often analyzed in the time-frequency domain. Besides, we present a novel two-step decoding procedure optimizing correlation between decoded information and ongoing behavior. Specifically, we apply machine learning methods to neuronal population activities recorded from the FEF, bilaterally, while monkeys performed a cued spatial target detection task. The FEF is an oculomotor structure located in the prefrontal cortex (Bruce et al., 1985; Bruce and Goldberg, 1985) that plays a central role in the control of spatial attention (Buschman and Miller, 2007; Ekstrom et al., 2008; Gregoriou et al., 2009; Ibos et al., 2013; Wardak et al., 2006). We report for the first-time (x,y) decoding accuracy (i.e.; a quantifiable continuous measure of accuracy) of attentional spotlight location from LFP signals. Confirming recent reports highlighting the contribution of gamma frequencies to attentional process (Fries et al., 2001; Gregoriou et al., 2009; Nandy et al., 2017; Paneri and Gregoriou, 2017; Richter et al., 2017), we further show that LFP attention-related informational content is greater in the gamma frequency band relative to lower frequency bands. The real-time attention decoding accuracies for LFP are comparable to what we achieved from MUA and are highly correlated with behavioral performance. Based on the observation that the (x,y) attention spotlight location estimated from both MUA and LFP signals correlate with behavior, we introduce a novel attentional position decoding method based on a distinction between trials with high and low attention related information content. We demonstrate that this procedure improves decoding accuracies obtained from LFP and MUA signals and importantly, improves their correlation with behavior. Overall, this study provides methodological bases to drive high attention-information content cognitive brain machine interfaces from both MUA or LFP activities. It also opens the way to targeting other cognitive functions such as working memory, and possibly extend this approach to non-invasive signals such as EEG or fMRI signals.

2. Methods

2.1. Subjects and surgical procedures

Two adult male rhesus monkeys (Macaca mulatta) were used in this experiment. All surgical and experimental procedures were approved by the local animal care committee (C2EA42–13–02–0401–01) in compliance with the European Community Council, Directive 2010/63/UE on Animal Care. The surgical procedures, the FEF location, and visual stimulation techniques have been described elsewhere (Astrand et al., 2016). Briefly, the FEF was defined as the anterior bank of the arcuate sulcus and we specifically targeted those sites in which a significant visual and/or oculomotor activity was observed during a memory guided saccade task at 10 to 15° of eccentricity from the fixation point. In order to maximize task-related neuronal information at each of the 24-contacts of the recording probes, we only recorded from sites with task-related activity observed continuously over at least 3 mm of depth.

2.2. Behavioral task

The task is a 100% validity endogenous cued spatial target detection task (Fig. 1A). The animals were placed in front of a PC monitor (1920 × 1200 pixels and a refresh rate of 60 Hz), at a distance of 57 cm, with their heads fixed. The stimuli presentation and behavioral responses were controlled using Presentation (Neurobehavioral systems®, https://www.neurobs.com/). To start a trial, the bar placed in front of the animal's chair had to be held by the monkeys, thus interrupting an infrared beam. The onset of a central blue fixation cross (size 0.7° × 0.7°) instructed the monkeys to maintain gaze position inside a 2° × 2° window, defined around the fixation cross. To avoid the abort of the ongoing trial, fixation had to be maintained throughout trial duration. Eye fixation was controlled thanks to a video eye tracker (Iscan™). Four gray square (size 0.5° × 0.5°) were displayed, all throughout the trial, at the four corners of a 20° x 20° hypothetical square centered onto the fixation cross. Thus, the four squares (up-right, up-left, down-left, down-right) were placed at the same distance from the center of the screen having an eccentricity of 14° (absolute x- and y-deviation from the center of the screen of 10°). After a variable delay from fixation onset, ranging between 700 – 1200 ms, a small green square, the cue (size 0.2° × 0.2°) was presented, for 350 ms, close to the fixation cross (at 0.3°) in the direction of one of the grey squares. Monkeys were rewarded for detecting a subtle change in luminosity of this cued square - i.e., the target. The change in target luminosity occurred unpredictably between 350 to 3300 ms from the cue off time. In order to receive a reward (drop of juice), the monkeys were required to release the bar in a limited time window (150 - 750 ms) after the target onset (hit trials). In order to make sure that the monkeys did use the cue instruction, on half of the trials, distractors were presented during the cue to target interval. Two types of distractors could be presented: (i) an uncued distractor (33% of trials with distractor) - that could take place equiprobably at any of the uncued locations; (ii) a workspace distractor (67% of trials with distractor) - that correspond to a small square presented randomly in the workspace defined by the four target locations. The contrast of the square with respect to the background was the same as the contrast of the target against the grey square. The monkeys had to ignore all of these distractors. Responding to any of them interrupted the trial. If the response occurred in the same response widow as for correct detection trials (150 - 750 ms), the trial was counted as a false alarm (FA) trial. Failing to respond to the target (Miss) similarly aborted the ongoing trial. Overall, data was collected for 19 sessions (M1: 10 sessions, M2: 9 sessions). The behavioral performance of each animal is presented in Fig. 1B (proportion of hits over miss and FA trials).

2.3. Recording techniques and data analyses

Bilateral simultaneous recordings in the two frontal eye fields (FEF) were carried out using two 24- contact Plexon U-probes (Fig. 1C). The contacts had an interspacing distance of 250 μm. Neural data was acquired with the Plexon Omniplex® neuronal data acquisition system. The data was amplified 400 times and digitized at 40.000 Hz. A threshold defining the multi-unit activity (MUA) was applied independently for each recording contact before the actual task-related recordings started, as follows. A first automatic step placed the threshold at mean+3*s.d. of the signal in time. A second step was sometimes required, involving a manual adjustment of the threshold. This second step was rarely needed and involved channels with sparse task-related MUA activity. Local field potentials (LFP) were recorded simultaneously on the same electrodes as MUA. The neuronal properties of the recorded neuronal sample have already been described elsewhere (Astrand et al., 2020; Gaillard et al., 2020). Supplementary figures S1 and S2 represent, for all trials, and sub-trial categories discussed in the main Fig. 4, average neuronal responses (Figure S1) and averaged time frequency spectra (Figure S2), for the preferred and non-preferred positions, aligned to cue and target presentation, across the 5 most responsive channels of each recording session.

2.4. Neuronal decoding procedure

All analyses were performed in Matlab 2017. MUA and LFP signals were aligned on the target presentation time and sorted according to the monkey's behavioral response (hits and misses). Fast Fourier transform analyses were performed on LFP signals recorded on each session, on each of the 48 channels in order to quantify the signal power spectrum from 1 Hz to 250 Hz. Specifically, each trial power spectrum was normalized using its own baseline calculated as the 300 ms prior to cue presentation power spectrum (fixation period). Time frequency analyses were performed using a hanning taper based on the fieldtripft_freqanalysis Matlab function (Oostenveld et al., 2011) with a

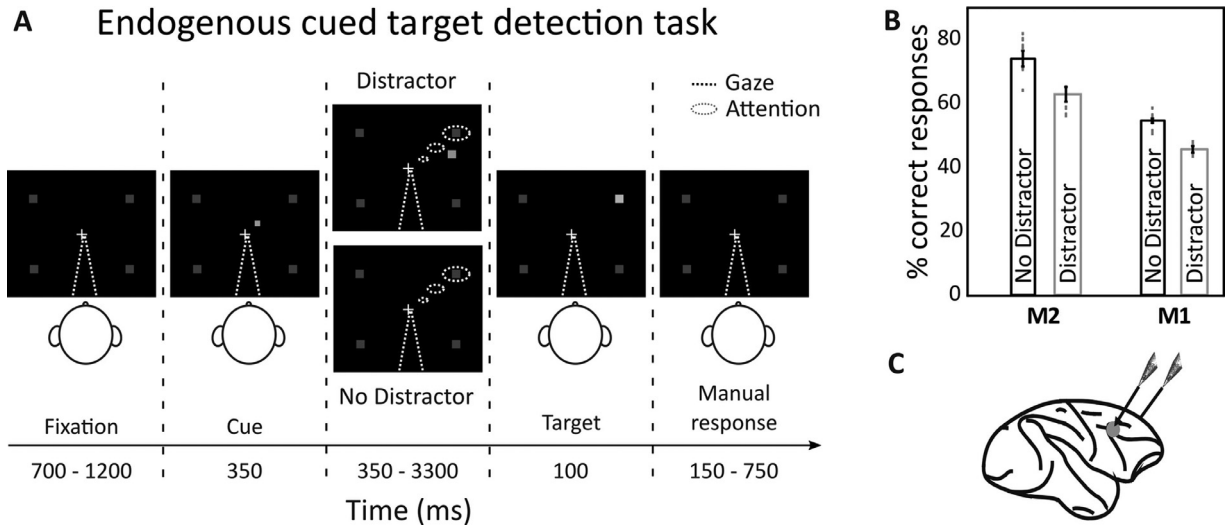

Fig. 1. ***Task design and behavioral performance.*** (A) 100% validity cued spatial target detection task with distractors. Monkeys had to hold a bar and fixate a central cross on the screen for a trial to be initiated. Monkeys received a liquid reward for releasing the bar 150 - 750 ms after target presentation. Target location was indicated by a cue (green square, second screen). Monkeys had to ignore any uncued event. (B) Behavioral performance of monkeys M1 and M2 at detecting the target in the presence or absence of a distractor (median% hits +/- median absolute deviations, dot correspond to individual sessions). (C) Recording sites. On each session, 24-contact recording probes were placed in each FEF.

fixed parameter of 7 cycles per time window (frequency dependent window length). Decoding from LFP signals was then performed either on unfiltered data or on eight independent frequency bands: δ (0–4 Hz), θ (4–8 Hz), α (8–12 Hz), low β (12–20 Hz), high β (20–30 Hz), low γ (30–60 Hz), mid γ (60–120 Hz), high γ (120–250 Hz). To avoid any border phase distortion effect or inter-frequency influences of filtering (Butterworth filter), we applied Fast-Fourier Transform algorithm on the raw detrended LFP data and isolated frequency bands of interest independently (and not from the full power frequency spectrum).

As in Astrand et al. (2016, 2015), a regularized linear decoder is used to associate, on hit trials, the neuronal activity with one of the four possible target locations. Specifically, this decoder is defined by the following equation: $C = W * (R + b)$, where C corresponds to the normalized (x,y) coordinates of the target (four possibilities: (1, 1), (1, −1),(−1,1),(1, −1)), W represents the weight matrix, R refers to the neuronal response (48-channel by N-trial matrix, corresponding to the average neuronal signal computed over the time interval of interest, for each of the 48 recording channels and each of the N training trials), and b is the bias. In order to avoid over-fitting, a Tikhonov regularization was used, defined by the following minimization equation: norm (W * (R + b) – C) + λ * norm(W). The scaling factor λ was chosen to allow for a good compromise between learning and generalization. During training, the decoder associated, on correct trials, the neuronal activity (R) to one of the four possible target locations (C) to calculate the corresponding weight matrix (W). Decoder input signals corresponded either to the number of spikes for MUA or to the normalized instantaneous power of all frequencies or specific frequency bands for LFPs, computed over the specified time window. On each given time interval before target presentation, the decoder was trained on a random set of 70% of hit trials and then tested on the 30% remaining hit trials and all misses, with activities sampled at the same interval as the training interval. Trial order were equalized in the training set to avoid any decoding bias. To avoid overfitting, training and testing were performed from different sets of trials. During training, the input of the classifier was a 48-channel by N-trial matrix, corresponding to the average neuronal signal computed over the time interval of interest as well as the normalized (x,y) coordinates of the target for each of these N training trials. During testing, for each trial, new to the classifier, the output of the classifier was estimated from a 48-channel vector corresponding to the average neuronal signal on the time interval of interest, on each of the 48 recording channels, on the considered testing trial. The output calculated by the decoder corresponds to an (x,y) coordinate. This output could either be used to assign attention to a specific visual quadrant, thanks to a hardlim function (i.e. a decoder output of (0.2, 1.2) could be assigned to the upper right quadrant, while a decoder output of (0.2, −0.1) would be assigned to the lower left quadrant), thus producing a classification readout (Astrand et al., 2014b, 2015). Alternatively, the output of the decoder, can be read as a spatial estimate of the locus of attention in the normalized decoding visual space (as in Astrand et al., 2016, 2020; Gaillard et al., 2020). Thus an output of (0.5, 0.6) estimates attention in the upper left quadrant, at a coordinate of (0.5, 0.6) in the normalized decoding visual space, irrespective of where attention was actually cued. These coordinates can be transformed in visual degrees by a simple linear transformation. Thus, for targets located at (10˚, 10˚), (−10˚, 10˚), (−10˚, −10˚), and (10˚, −10˚), the attention readout in this specific case would be (5˚, 6˚). Training and testing were performed on neuronal signals from 10 ms to 1200 ms before target presentation with a time step of 20 ms. Indeed, on such trials, the neuronal activities aligned onto target presentation can be analyzed on the longest 1200 ms windows without the risk of contamination of the attention-related information on or off cue-related neuronal responses. All trials with cue-to-target intervals shorter than 1700 ms were excluded from this analysis. For each interval, training and testing steps were repeated 100 times, then averaged to define a decoding performance corresponding to the number of correct classifications according to quadrant categories. We estimated the 95% confidence interval to verify the statistical significance of our decoding performance. The same decoding analyses as described above were used with a training set based on random labels. In other words, the decoder used the same neuronal signal, but the coordinates of the target were randomized and thus did not correspond to the actual condition in which the neuronal signal was recorded.

On each given time interval before target presentation, the decoder is trained on a random set of 70% of hit trials (mean = 765, s.e. = 35) and then tested on the 30% remaining hit trials (mean = 328, s.e. = 15) and all misses (mean = 657, s.e. = 81), with activities sampled from the same interval as the training interval. The (x,y) location of the attentional spotlight is calculated from a leave-one-out decoding strategy (i.e., training was performed on all hit trials (mean = 1093, s.e. = 51) except one, used for the testing). For misses, the decoder is trained on all

hit trials (mean = 1094, s.e. = 51) and tested on all misses (mean = 657, s.e. = 81).

Importantly, all decoding procedures were applied independently for each session and each subject. Indeed, recordings were performed on a daily session basis, at different FEF cortical locations. As a direct result of the spatiotopic organization of the FEF (Bruce et al., 1985; Bruce and Goldberg, 1985), each different electrode location resulted in a different set of weights (W) associating recorded neuronal activity to attentional position. Therefore, cross subject/session decoding procedure produces very low decoding performances.

2.5. Behavioral correlation

In order to validate the decoding procedure, we investigated the correlation between the (x,y) attentional spotlight decoded from neuronal signals with monkey's behavioral response (Percentage of hits over hit+miss trials). Specifically, the relative distance between the actual target location and the decoded attentional spotlight location was calculated for each trial. Percentage of hits over miss trials was then calculated over 0.5° distance vectors. To avoid biases, total number of hits and misses were equalized and then binned - the whole procedure was repeated 100 times. The X and Y location of attentional spotlight was calculated from a leave-one-out decoding strategy (i.e., training was performed on all hit trials except one used for the testing). For misses, the decoder was trained on all hit trials and tested on all misses. Training and testing were performed on a 150 ms time window prior to target presentation. Statistical analyses were carried out using linear regression model.

2.6. Two-step decoding procedure

In this part, we dissociate high attention-related informational spatial content trials from low attention-related informational content trials. We use the relative distance calculated between the decoded (x,y) attentional spotlight (AS) and the real target location (T) for hit trials, as described above. Two categories of hit trials were identified from this first decoding: 1) trials in which the decoded attentional spotlight is close to target location (i.e. HighContent trials) and 2) trials in which the decoded attentional spotlight is far from target location (i.e. LowContent trials). HighContent and LowContent trials were defined according to a threshold of 7° between real target location and decoded attentional spotlight (HighContent trials: $|AS\text{-}T| < 7°$; LowContent trials: $|AS\text{-}T| \geq 7°$). Given the high difficulty of the task, monkeys cannot succeed in the trial if they are not orienting their attention near to the target location (Astrand et al., 2016). Thus, we hypothesized that these differences between HighContent and LowContent trials was due to differences in spatial attention informational content between these two types of hit trials, and that signals were more representative of the expected target location in HighContents trials than in LowContent trials. Decoding performance and behavioral correlation were thus calculated a second time as follows. In order to evaluate classification performance, training was performed on all HighContent trials and testing was performed on different percentages of HighContent trials over LowContent trials (0% to 100% ratio). The proportion 70/30 of trials used for training and testing was conserved. Once training and testing sets were selected, the decoding procedure applied was the same as the procedure described in the previous section. In order to evaluate the correlation between decoded attention position and behavioral performance, we performed a trial by trial (x,y) estimation of attentional position. More specifically, for HighContent trials position decoding, the decoder was trained on all HighContent trials except one and tested on the remaining one (leave one out strategy). For LowContent trials and misses, the decoder was trained on all HighContent trials and tested on LowContent trials and misses. Training and testing were performed 150 ms before target presentation. The relative distance between AS and T was calculated and associated with the percentage of hit trials with respect to misses. Hit trials included 50% of LowContent trials and 50% of HighContent trials. For each signal (MUA and LFP), we compared the effect of HighContent trials on decoding performance and behavioral correlation. Statistical comparisons were performed using non parametric tests (Wilcoxon rank sum test) and linear regression models (F-tests).

3. Results

In order to access the location of the attentional spotlight, a linear decoder was used to estimate the (x,y) coordinates of attention based on MUA and LFP signals, recorded from the prefrontal cortex (FEF, bilaterally, Fig. 1C) while monkeys performed a cued target detection task (Fig. 1A). The readout of this linear decoding procedure can be classified in one of four possible classes indicating whether attention is correctly oriented to the cued visual quadrant (correct classification), or to one of the three other quadrants (incorrect classification, Astrand et al., 2014, Tremblay et al., 2015). Alternatively, the readout of the linear decoding can be taken as an error to the cued location and transformed into an (x,y) continuous coordinate (Astrand et al., 2020, 2016; Gaillard et al., 2020). In the first part of the results, we report for the first time continuous attentional spotlight position decoding from LFP signals, with performance accuracy levels similar to MUA based decoding. We then analyze how the continuous (x,y) estimates of attentional spotlight based on prefrontal MUA and LFP signals predict behavioral performance, thus validating the decoding procedure. Finally, we develop a decoding method that optimizes the spatial decoding of attention from MUA and LFP signals and highlights qualitative variability in prefrontal attention related information.

3.1. Classifying spatial attention from prefrontal MUA and LFP

Fig. 2A and B represent the classification performance based respectively on FEF recorded MUAs and LFPs (irrespective of frequency content). Neuronal activity (decoder input) was averaged just prior to target presentation, calculated across varying time windows ranging from 10 ms to 1200 ms. Decoding accuracy on hit trials is significantly higher than chance level (25%) and higher than the 95% confidence interval (Fig. 2, light blue curves) for both MUA (Fig. 2A, blue, significance represented by the black line) and LFP signals (Fig. 2B, blue, significance represented by the black line). Thus, on hit trials, spatial attention can be successfully classified from both MUA and LFP signals. It is worth noting that attention decoding accuracy is only partially (though statistically significantly) degraded when considering channels from only the ipsilateral FEF relative to the contralateral FEF (supplementary figure S3). This is probably due to two specificities in the FEF receptive field properties (Bruce and Goldberg, 1985; Bruce et al., 1985). First, these receptive fields often expand into the ipsilateral visual hemifield. Second, visual stimuli, as well as spatial attention oriented in the ipsilateral visual hemifield often evoke inhibitory neuronal responses. This information appears sufficiently precise for the decoder to extract information about spatial attention including in the ipsilateral visual field.

Interestingly, decreasing time intervals before target presentation highly impacts decoding accuracies. Performances decrease from 77% to 40% for MUA (Fig. 2A, blue, Wilcoxon rank sum test, $p < 0.05$) and from 71% to 29% for LFPs (Fig. 2B, blue, Wilcoxon rank sum test, $p < 0.05$). Compared to short time windows, longer time windows reflect average spatial attention location, and thus yield higher classification rates. On both signals, window size thus implies a trade-off between temporal resolution and overall classification accuracy.

While MUA signals are processed in the time-amplitude domain, LFP signals are processed in the time-frequency domain. In the following part, we segregated the different functional frequency bands of LFPs to investigate their specific impact on classification performances. Fig. 2C represents the decoding accuracy in time as a function of specific LFP functional frequency band content. As observed on the overall decoding accuracy from all LFP frequency content decomposition, larger window

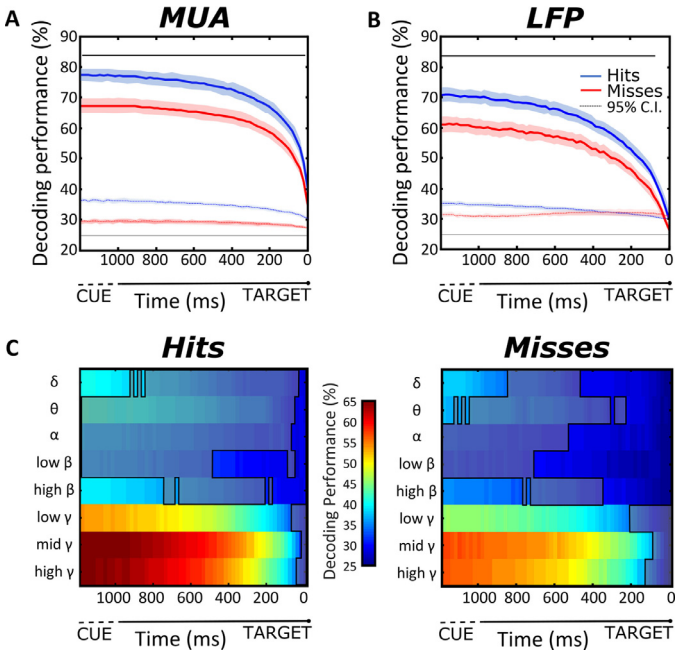

Fig. 2. ***Spatial attention decoding accuracies*** from (A) multi-unit activity (MUA) or (B) local field potentials (LFP), as a function of averaging time window size from target onset (0 ms), on hits (blue, mean +/- s.e.) and miss trials (red, mean +/- s.e.). Black dashed line (25%): absolute chance level; dashed blue and red curves: 95% C.I. for hit and miss trials. (C) Spatial attention decoding accuracy from LFP signals per LFP frequency band, as a function of averaging time window size from target onset (0 ms), on hit (left) and miss trials (right). Shaded gray area: no significant difference in performance as assessed by a Wilcoxon rank sum test (M1: 10 sessions, M2: 9 sessions).

sizes yield higher decoding accuracies in all frequency bands (Fig. 2C). However, information about spatial location of attention is mainly contained in the gamma frequency bands (30–250 Hz). Specifically, on hit trials, for the largest window sizes, decoding accuracies are below 50% for all frequency bands < 30 Hz (δ = 40%; θ = 42%; α = 36%; low β = 35%; high β = 39%) and reach a maximum of 54% for low γ (30–60 Hz), 66% for mid γ (60–120 Hz) and 65% for high γ (120–250 Hz, Fig. 2C). Specifically, decoding performances were not significantly higher than 95% CI for the θ, α and low β bands. In addition, full spectrum LFP decoding accuracy is statistically higher than each LFP band-specific decoding accuracies, except for the mid gamma frequency band from which it is statistically undistinguishable (supplementary figure S4B, Wilcoxon rank sum test, $p < 0.05$)

In order to quantify the level of attentional information shared by the selected frequency bands of interest, we analyzed the correlation between decoded (x,y) positions for each frequency pair (δ, Θ, α, low β, high β, low γ, mid γ, high γ, and full LFP spectrum, figure S5, Spearman correlation coefficient, n = 20,778 trials, 19 sessions). This analysis reveals significant correlations between attentional (x,y) position decoded across the lower frequency bands (δ & Θ (corr. coef. 0.641, $p < 0.001$), Θ & α (corr. coef. 0.654, $p < 0.001$)) as well as across the higher frequency bands (mid γ & high γ (corr. coef. 0.551, p <0.001), mid γ & full LFP (corr. coef. 0.733, $p < 0.001$), high γ & full LFP (corr. coef. 0.8653, $p < 0.001$)). Overall, this indicates some level of dependency in attention-related information within these groups of frequency bands.

For both MUA and LFP signals, decoding is significantly more reliable on hit trials than on misses at all window sizes (e.g. window size = 1200 ms, MUA: Fig. 2A, blue, mean = 77%, s.e. = 2.1% vs. red, mean = 67%, s.e. =2.4%; LFP: Fig. 2B, blue, mean = 71%, s.e. = 2.1% vs. red, mean = 61%, s.e. = 2.4%, Fig. 2, Wilcoxon rank sum test, $p < 0.05$). This holds true for all LFP frequency bands, although impact of negative trial outcome is stronger on higher LFP frequency bands as compared to lower (Fig. 2C, supplementary figure S4A). Overall, this supports that spatial attention is miss allocated during miss trials (Astrand et al., 2016; Gaillard et al., 2020), subsequently interfering with perception (Astrand et al., 2020).

3.2. The decoded (x,y) attentional spotlight predicts behavior

In order to validate attentional decoding procedure, correlations between decoded positions and subjects' behavioral performances were investigated. In the following, attention to target distance is defined, in each trial, as the distance between expected target location and the corresponding decoded (x,y) attentional spotlight, 150 ms before target onset. This distance parameter is then correlated to a behavioral performance calculated as the percentage of hits over hit+miss trials. For all signal types, we observe that monkeys produce more hits when their attentional spotlight is deployed closer to target location. Specifically, we demonstrate a significant linear correlation between the distance of decoded attentional spotlight to target and the hit rate, when using MUA based decoding (Fig. 3A. linear regression: $r^2 = 0.48$, $F = 86$, p-value < 0.005) as well as when using LFP based decoding (Fig. 3.B linear regression: $r^2 = 0.65$, $F = 174$, p-value < 0.005). This observation is reproduced on reaction times, such that, reaction times are significantly shorter when the MUA-based attentional spotlight is closer to the target (supplementary figure S6A). This also hold true to the LFP-based attentional spotlight (supplementary figure S6B). This indicates that similarly to MUAs, LFPs spatial attention information predicts behavior.

In order to better understand which frequency bands held the most reliable spatial information, the above described correlation analysis is reproduced for each independent functional LFP frequency band (Fig. 3C). Overall, correlations are weak for the lower frequency bands and increase for the higher frequency ranges (Fig. 4C: δ: $r^2 = 0.18$, $F = 0.0$, p-value < 0.005/ θ: $r^2 = 0.13$, $F = 0.0$, p-value < 0.005/ α: $r^2 = 0.26$, $F = 0.0$, p-value < 0.005 / low β: $r^2 = 0.13$, $F = 0.0$, p-value < 0.005/ high β: $r^2 = 0.17$, $F = 0.0$, p-value < 0.005/ low γ: $r^2 = 0.29$, $F = 0.0$, p-value < 0.005 / mid γ: $r^2 = 0.42$, $F = 0.0$, p-value < 0.005 / high γ: $r^2 = 0.40$, $F = 59.3$, p-value < 0.005).

These analyses bring about two important observations. First, spatial attention LFP-based decoding correlates with behavior to the same extent as MUA-based decoding. Second, this is mostly due to the gamma frequency LFP power content.

3.3. Optimizing (x,y) access to attentional spotlight using a two-step decoding procedure

From the above correlation between decoded attentional spotlight distance to expected target location and hit rate, we observe that for a proportion of hit trials, the decoded (x,y) attentional spotlight is estimated close to the expected target location, while for the rest of the trials, the decoded attentional spotlight is estimated far away from the expected target (Fig. 4A). Based on the observation that decoded location accounts for behavior, we reasoned that when training our decoder on hit trials, we are actually training it on suboptimal conditions, presenting it with both trials in which attention is close to the expected target location, and trials in which attention is farther away. We thus here define two different categories of trials: HighContent trials (Fig. 4A), defined by decoded attentional spotlight to expected target distance inferior to 7° and LowContent trials (Fig. 4A), defined by decoded attentional spotlight to expected target distance superior to 7° Please note that this nomenclature does not assume in any way that the decoder is fully capturing all attention-related information. Rather it is assuming that this information is, on some trials, better captured than on others. Supplementary figures S1 and S2 represent, for all trials, as well as for HighContent and LowContent sub-trial categories, average neuronal responses (figure S1) and average time frequency spectra (figure S2), for the preferred and non-preferred positions, aligned to cue and target presentation, across the 5 most responsive channels of each recording

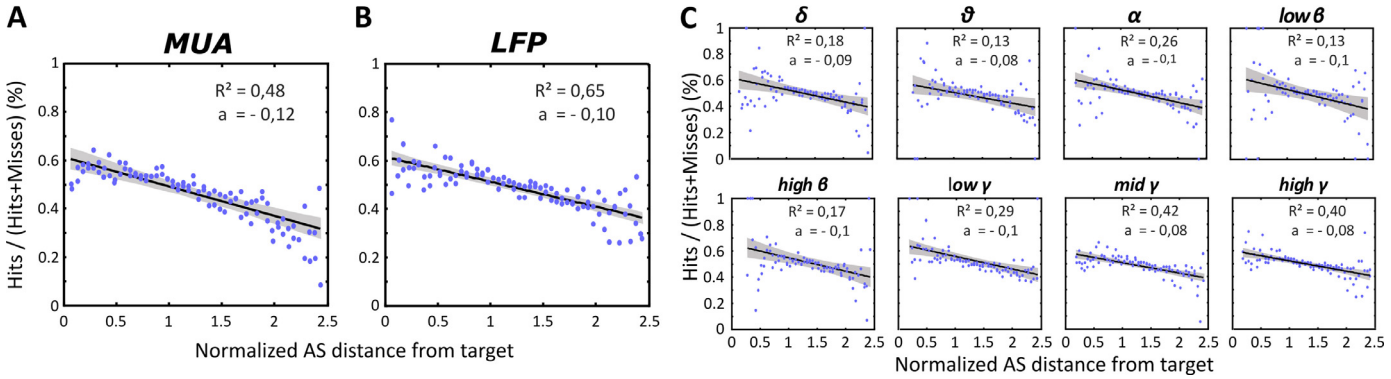

Fig. 3. ***Correlation between behavioral performances & distance between the attentional spotlight and the target location*** estimated from (A) multi-unit activity (MUA), (B) local field potentials (LFP), on all frequency power content or (C) as a function of specific frequency ranges ((δ (0–4 Hz), θ (4–8 Hz), α (8–12 Hz), low β (12–20 Hz), high β (20–30 Hz), low γ (30–60 Hz), mid γ (60–120 Hz), high γ (120–250 Hz)). Blue dots: binned data points; black line: best linear fit; gray shaded area: 95% C.I. F and p-values are indicated in the main text. Behavioral performance, y-axis: ratio between hit and hit+miss trials in%. Distance between the decoded attentional spotlight (AS) and actual target presentation location, x-axis: normalized distance. (M1: 10 sessions, M2: 9 sessions).

session. The decoder captures the difference in population information content between these two categories of trials from both MUAs and LFPs.

In a first analysis, all decoders are trained on exclusively HighContent trials. As predicted by the rationale behind dividing trials on HighContent and LowContent attentional trials, testing the decoder on varying proportions of HighContent trials relative to LowContent trials critically impacts spatial attention decoding performance. Using 100% HighContent trials testing set from MUA signal leads to an average increase in decoding of 27% (s.e. = 0.8%) between 10 ms to 600 ms pre-target averaging window sizes and an average increase of 18.7% (s.e. = 0.3%) between 600 ms to 1200 ms pre-target (Fig. 4B, Wilcoxon rank sum test, p-value < 0.05) relative to a regular decoding procedure involving only step one. Using 100% HighContent trials testing set from LFP signal leads to an average increase in decoding of 34% (s.e. = 0.9%) and 25% (s.e. = 0.7%), respectively for the short and long pre-target averaging window sizes (Fig. 4B, Wilcoxon rank sum test, p-value < 0.05). This effect was particularly striking for smaller window sizes. A significant increase of performances with respect to a randomly distributed dataset is observed for a minimum threshold of 70% of HighContent trials in the MUA testing set and 50% in the LFP testing set (Fig. 4B, Wilcoxon rank sum test, p-value < 0.05). In addition, and in contrast with what is described in Fig. 2, decoding accuracy increment is most marked for shorter than for longer time intervals. Overall, the higher the HighContent testing trials rate, the higher the gain in attention classification performance. In contrast, the higher the LowContent testing trials rate, the higher the loss in overall spatial attention decoding performance. A testing set of 100% LowContent trials leads to a drastic reduction of decoding performance compared to a randomly distributed testing set both for MUA signals (Fig. 4B, −13% (s.e. = 0.4%) between 10 ms to 600 ms and −16% (s.e. = 0.1%) between 600 ms to 1200 ms, Wilcoxon rank sum test, p-value < 0.05) and LFP signals (Fig. 4B, −10% (s.e. = 0.8%) and −12% (s.e. = 0.6%), Wilcoxon rank sum test, p-value < 0.05). A significant decrease in spatial attention decoding accuracy as compared to a random training dataset is observed for MUA (resp. LFP) testing sets starting from 80% or more LowContent trials (resp. 90%, Fig. 4B, Wilcoxon rank sum test, p-value < 0.05). Thus, LowContent trials are detrimental to spatial attention decoding accuracy. Importantly, the positive effect of HighContent testing trials on decoding performance is more marked for LFP signals than MUA signals (Wilcoxon rank sum test, p-value < 0.005). Moreover, LFP signals are less impacted by the lower ratios of HighContent trials over LowContent trials than MUA signals - thus resulting in a lower decrease in decoding performance (Wilcoxon rank sum test, p-value < 0.005). In other words, while the two-step decoding improves attention decoding accuracies, this impact is more pronounced on LFP signals than on MUAs.

In order to assess the impact of the proportion of HighContent trials relative to LowContent trials in the training set, we further estimated, for neuronal activities averaged over 150 ms prior to target presentation, the decoding accuracies obtained for varying HighContent vs. LowContent trials in both the training and testing sets (supplementary figure S7). Overall, both ratios were critical to optimal decoding performance. However, confirming the logic of the proposed two-step decoding, overall decoding accuracies are highest (figures S7AC) and significantly above the standard decoding accuracies (figures S7BD), for both MUA and LFP signals, when HighContent trial proportion is high in both the training and testing sets. In mirror to this, overall decoding accuracies are lowest and significantly below the standard decoding accuracies when LowContent trial proportion is high in both the training and testing sets (figure S7).In particular, when training is performed exclusively onto LowContent trials, no information can be recovered from novel testing trials, including when testing is performed on HighContent trials, most probably due to the fact that on LowContent training trial sets, decoded attention location is uncorrelated with cue instruction. As a result, no learning can take place. Overall, this confirms that prior selection of a spatial information rich training dataset is crucial to optimize access to prefrontal attentional encoding and further improve classification performances on remaining trials.

Functional validity of this two-step decoding procedure implies that exclusive training on HighContent trials, whether in MUA or LFP signals, maximizes the correlation between the decoded attentional spotlight to expected target distance and behavioral performance (Astrand et al., 2016). We thus trained a decoder using only HighContent trials and tested it on misses and remaining HighContent trials (50% of hit testing trials) and LowContent trials (50% of hit testing trials) to simulate a balanced proportion of hit trials categories and misses. As expected, HighContent trials based decoding increases the linear relationship between attentional spotlight to target distance and behavioral performance. Specifically, in the MUAs, r^2 value increased from 0.48 (Fig. 3A linear regression: $r^2 = 0.48$, $F = 85.8912$, p-value < 0.05) to 0.91 (Fig. 4C, linear regression: $r^2 = 0.91$, $F = 962$, p-value < 0.005), and correlation slope becomes markedly more steep (Fig. 4C, linear regression: $a = -0.3$, vs. Fig. 3A linear regression: $a = -0.12$). In the LFPs, r^2 values increase from 0.65 (Fig. 3B linear regression: $r^2 = 0.65$, $F = 174$, p-value < 0.005) to 0.86 (Fig. 4D linear regression: $r^2 = 0.86$, $F = 569$, p-value < 0.005), and correlation slope also becomes steeper (Fig. 4D linear regression: $a = 0.27$, vs. Fig. 3B linear regression: $a = 0.10$). Overall, this thus confirms the functional validity of this two-step decoding procedure, both for MUA-based decoding of spatial attention, as well as for LFP-based decoding of spatial attention. Crucially, we demonstrate that using spatial information enriched trials (i.e. HighContent trials)

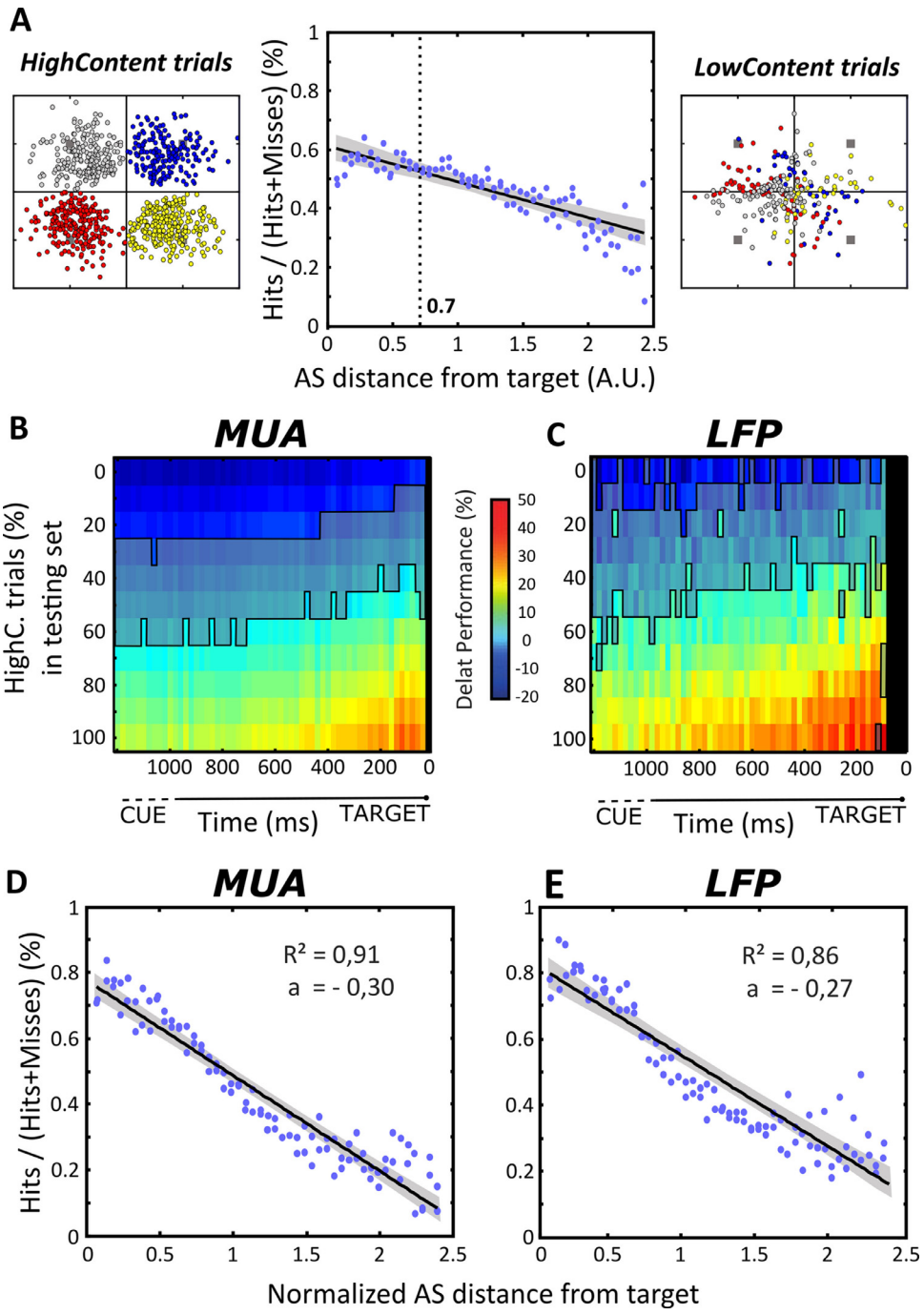

Fig. 4. ***Two-step decoding procedure improves correlation between behavioral performance & distance between the attentional spotlight and the target location.*** (A) Following the first decoding step, hit trials can be subdivided into HighContent and LowContent trials based on how close decoded attentional spotlight is to the actual target location (mid panel). HighContent trials consistently fall in the cued quadrant (left panel) while LowContent trials don't. Note that the tendency of decoded attention to over-explore the center of the screen on LowContent trials can be attributed to the fact that attention is dynamic and globally has a higher probability to sample the portion of the screen lying more central to the expected target location rather than more peripheral. Alternatively, this can be due to the fact that attention is not properly focused in a spotlight fashion. (B-C) Following the second decoding step, the higher the proportion of HighContent trials in the testing set, the higher the attention decoding accuracy on novel trials. This improvement in attention decoding accuracy is more marked when decoding from LFP signals (C) than from MUA signals (B) (HighContent trials (HighC.); LowContent trials (LowC.); Shaded gray are: no significant difference in performance as assessed by Wilcoxon rank sum test; Shaded black are: time intervals excluded due to absence of HighContent trials for 5 sessions). (D-E) This two-step decoding procedure improves the correlation between overt performance (Hits/Hits+Misses) and the distance of the decoded attentional spotlight (AS) to the target location (Higher R^2, steeper slope) for both MUA signals (D) and LFP signals (E). (M1: 10 sessions, M2: 9 sessions).

allows to better account for the relationship between observed behavior and the (x,y) decoded attentional spotlight.

4. Discussion

In this manuscript we report for the first time high decoding accuracy of the (x,y) location of the attentional spotlight based on prefrontal LFP signals, to a comparable degree to that achieved from MUA signals. We show that both decoded information (MUA and LFP signals) are predictive of behavioral content and that LFP attention-related information is maximal in the gamma band. In addition, we show that selecting maximally attention-informative trials (HighContent trials) during the decoding procedure strongly improves the correlation between our MUA and LFP based decoding and behavioral performance, thus further refining the functional relevance of this decoding of the (x,y) locus of the attentional spotlight. This improvement is more marked for LFP signals than for MUA signals. In the following, these findings are discussed in the light of the current literature.

4.1. Decoding attentional information from LFP signals

The neural bases of spatial attention in the prefrontal cortex have been extensively studied based both on neuronal spiking activity, local field potentials and interferential studies (Ibos et al., 2013; Buschman and Miller, 2007; Wardak et al., 2006). In recent years, this accumulated knowledge has set the grounds for real time decoding of attention both from invasively recorded spiking activity (Astrand et al., 2014a, 2016, 2020; Farbod Kia et al., 2011; Gaillard et al., 2020;

Tremblay et al., 2015) and non-invasive brain signals (Andersson et al., 2011, 2012; Thiery et al., 2016; van Gerven and Jensen, 2009). Attentional decoding methods from MUA signal have made substantial progress, moving from the classification of attention into subspace sectors to the actual decoding of the (x,y) position of the attentional spotlight (Astrand et al., 2016; Tremblay et al., 2015). However, progress has been much slower in the decoding of attention from non-invasive MRI or EEG signals. Decoding of attention from LFP signals and developing novel decoding strategies on this type of signals can be considered as an intermediate step towards improving the decoding of attention from less invasive signals.

To our knowledge, only one study to date has addressed the decoding of spatial attention from prefrontal LFP, based on a four spatial quadrant classification approach (Tremblay et al., 2015). Here, we report, for the first time the real-time tracking of the (x,y) attentional spotlight locus from prefrontal LFPs. Crucially, we show that the extracted (x,y) locus of the attentional spotlight is highly predictive of the behavioral performance, such that the closer the attentional spotlight to the target presentation location, the higher the correct detection rate. In contrast, the further away the attentional spotlight to the target presentation location, the higher the miss rate. This is important in two ways. First, this result validates the behavioral relevance of the decoding procedure, describing a direct behavioral relationship between where the decoded attentional spotlight is in space relative to where the target is presented and the detection rate of the subject. Second, this indicates that very much like has been described from MUA-based attentional spotlight tracking, the LFP-based attentional spotlight is highly dynamic and explores space even when cued towards a specific location. Indeed, the LFP-based decoded attentional spotlight is not anchored at the expected target location following cue presentation, but can be more or less close to this task-relevant location, in spite of the fact that behavioral performance is enhanced when the attentional spotlight is closest to the cued location.

As previously described by Tremblay et al. (2015), we confirm that attention-related information is maximal in the LFP gamma frequency band (above 30 Hz, and maximally between 60 and 120 Hz). Attention-related information can still be extracted above chance in lower LFP frequency bands, though at much lower accuracies. These results are in agreement with the contribution of gamma frequency bands to attentional processes. Indeed, in V1, attention is shown to selectively decrease LFP gamma synchronization as well as gamma spike field coherence, in the low gamma band (Chalk et al., 2010). In contrast, attention orientation enhances low gamma synchronization and perception in V4 (Fries et al., 2001), and enhances low gamma band oscillatory coupling between the FEF and V4 (Gregoriou et al., 2009). This indicates that gamma mechanisms are different across cortical areas. Within the FEF, a strong phase-amplitude coupling is observed in the LFP theta content and the low gamma band during attention orientation (Fiebelkorn et al., 2018). Most of these studies highlight the long range functional role of low gamma band. Only few studies have addressed the distinctive functional contribution of low gamma band ($\leq$ 60 Hz) relative to higher gamma band LFP content (mid and high gamma in our analyses). Several hypotheses are proposed to address the function of these high gamma rhythms in attentional process. Recording from the somatosensory cortex, Ray et al. (2008) elegantly show that high-gamma power in the LFP strongly correlates with the average spiking firing rate, both in time and on a trial-by-trial basis. In contrast, the correlation between firing rate and low-gamma power (40–60 Hz) is much smaller. Using a modelling approach, the authors show that high-gamma power is more sensitive to changes in spiking rate than to changes in neuronal synchrony. More recently, Leszczyński et al. (2020) show that, in primary visual cortex V1 and primary auditory cortex A1, high gamma can be divided into two independent components, a deep and a superficial component, only the former being strongly associated with MUA activity. This thus suggests that the second component reflects dendritic processes that are dissociable from local neuronal firing. This most probably accounts for the fact that the attention decoding accuracies from the mid gamma band power is indistinguishable from the decoding accuracies from average LFP frequencies. Interestingly, attention-related information can still be extracted above chance in lower or higher LFP frequency bands, though at lower accuracies. Therefore, from a methodological point of view, there is no benefit in decoding attention-related information from specific independent frequency bands. Indeed, average power LFP decoding accuracy is higher or equal to gamma specific LFP power. Overall, this result suggests that attention related information is not fully redundant across frequency and stresses the notion of functional rhythms (Fries, 2015; Gaillard et al., 2020).

The correlation between decoding and behavior is further enhanced using the two-step decoding procedure that we introduce here and that is discussed below. This latter point is crucial for neurofeedback and cognitive brain-machine interfaces (Andersen et al., 2010; Astrand et al., 2014b; Enriquez-Geppert et al., 2017; Jiang et al., 2017; Ordikhani-Seyedlar et al., 2016), where one wants to work with information of maximal behavioral relevance. Interestingly, Salari et al. (2014) demonstrate a modulation of perception by a neurofeedback manipulation based on EEG gamma power. This is possibly in agreement with our observation that gamma frequency contains high attention-related information. However, these studies are based on direct modulation of surface gamma power, independently from behavioral performance or a global extraction of attentional spotlight locus. Our approach allows to track the dynamic attentional spotlight with a high temporal resolution (down to 30 ms). We expect this type of approach to provide subjects with more informative and reliable neurofeedback to work on.

4.2. Comparing to EEG studies

Several studies both in humans and non-human primates report access to a two or a four quadrant classification of subject's attention location while performing a simple cognitive task with eyes fixed (Andersson et al., 2011; Astrand et al., 2014a, 2014b; Rotermund et al., 2013; Tremblay et al., 2015; Zhang et al., 2011). Brain activity decoding approaches have been applied to numerous signal types, ranging from EEG (Morioka et al., 2014; O'Sullivan et al., 2015; Treder et al., 2011; van Gerven and Jensen, 2009) to ECoG (Gunduz et al., 2012) and fMRI (Andersson et al., 2012, 2011). In particular, the EEG literature, has followed two distinct approaches at decoding visuospatial attention. The first one is based on the decoding of occipito-parietal ERP amplitude in the presence or absence of attention. This has led to the development of such tools as the P300 Speller tool as well as to the exploration of the temporal dynamics or goal-relevant representations (Hubbard et al., 2019). It is important to note that this approach does not allow to track covert attention *stricto sensu*, as it relies on the interpretation of the modulation of the response to a visual probe, which can be attended or not attended. The second approach is based on an actual tracking of covert attention, mostly based on the topographical organization of the power of the occipito-parietal alpha band (Samaha et al., 2016). Desantis et al. (2020), additionally show that alpha power is more associated with the orientation of covert attention in space, while raw EEG activity is more associated with the influence of attention on perception. Likewise (Bae and Luck, 2018) show that alpha band oscillations primarily carry information about spatial attention orientation, while sustained potentials carry information about the information held in working memory.

Most of these EEG studies rely on occipito-parietal alpha. In monkeys, converging evidence suggest that the prefrontal cortex (PFC), and specifically the frontal eye fields (FEF) is at the origin of attentional spotlight control, gating neuronal activity in the parietal and occipital cortex (Buschman and Miller, 2007; Ekstrom et al., 2008; Gregoriou et al., 2009; Ibos et al., 2013; Wardak et al., 2006), the PFC controlling attentional modulation of alpha and gamma oscillations in lower order cortical regions (Fiebelkorn et al., 2018; Kerkoerle et al., 2014; Kienitz et al., 2018). While accessing precise attention-related information from the

prefrontal cortex might remain challenging using EEG recordings, due to the intrinsic properties of this methodology, targeting prefrontal attention information actually has major advantages over decoding occipital information. The first important advantage is, as described above, the fact that PFC the source of attentional orientation signals. Attention-related signal-to-noise ratio in that region is thus expected to be higher than in down-stream regions. In addition, and actually related to the previous point, occipital alpha power is not of unique origin, but should be considered as a compound signal, arising from the influence of multiple cortical (Gregoriou et al., 2009; Kerkoerle et al., 2014; Kienitz et al., 2018) and subcortical sources (Saalmann et al., 2012). This difference between prefrontal and occipital attention-related information is important for decoding applications. It however becomes crucial in neurofeedback applications, whereby targeting prefrontal attentional processes are expected to have a stronger behavioral influence than targeting compound occipital processes.

4.3. Exploiting attention dynamics to improve real-time attention decoding accuracies

There is a crucial need in the field of machine learning to develop methods to isolate a small set of critical samples (referred to as representative dataset) that best describes an unknown process. Several recent studies in the machine learning field report high increase in classification performances using re-training procedures based on sub data-set (Kitamura and Deible, 2020; Niu et al., 2020), as proposed here. Indeed, it has been shown that huge training data libraries used to train decoders to dissociate between multiple features, while allowing to avoid over-fitting, may actually lead to under-fitting. In contrast, small specific subsets of training data prevent under-fitting while not necessarily leading to over-fitting if well designed. In addition, one important limitation to huge training datasets is the cost of building such labelled libraries. This cost turns out to be crucial when dealing with physiological data of high intrinsic variability (as compared to dataset that can be labelled automatically, such as pictures or words for instance). Recent studies report that training dataset size can be compressed by up to 95% without any drop in classification performance, by identifying “representative samples” in the training dataset (i.e. high informational content trial) (Ghadikolaei et al., 2019). This is very similar to the two-step decoding procedure proposed here.

The fact that the attentional spotlight is extremely dynamic (Gaillard et al., 2020) suggest that not all hit trials are equivalent. Indeed, we observe that some hit trials take place when the attentional spotlight is successfully located where the target appears and other hit trials in contrast happen when attention is far away from target presentation location. This has a direct impact on decoding performances. The more space sampled, less stable the information in the neuronal population, thus impairing resulting decoding performance. On the contrary, a trial with less exploration and a more stable spotlight will lead to a stable neuronal information and more accurate decoding. Based on these observations, we reasoned that training our classifier on all of these hit trials is suboptimal as compared to training the classifier on hit trials in which attention was properly oriented. We thus use a first decoding step to identify such good trials (i.e., high attention-related information content or HighContent trials) and specifically use them to train the decoder on a second decoding round. This significantly increases the attention decoding accuracies. Several points need to be noted. First, as expected from our initial hypothesis, the higher the proportion of HighContent trials used for the training the higher the relative gain in decoding accuracies. Strikingly, for both MUA and LFP signals, decoding improvement is higher when considering short time interval compared to longer time window. This observation could be explained by the fact that the longer the time window, the more attention is expected to explore the target position, this both on HighContent and LowContent trials. Quite importantly, this increment in decoding accuracies was more marked for the LFP decoding than for the MUA decoding. This possibly indicates that LFP signals multiplex attention related information with other sources of information, contributing to LFP signal variability, and that are more prevalent on LowContent than on HighContent trials. Last but not least, this two-step decoding procedure drastically improves the correlation between the (x,y) attentional spotlight real-time estimate and behavioral performance, whether from MUA or LFP signals. In other words, the decoded attentional spotlight better explains behavior, both as assessed from the strength of the correlation and from its slope. The real-time performance of the decoder is impacted by two main factors: the neuronal averaging window and the test time (usually less than 5 ms). In the case of neurofeedback applications, an additional communication cost between the processing hardware and the presentation hardware must be added (typically in the range of 10 to 70 ms, depending on multiple technical parameters). An important aspect of this two-step decoding is that it doesn’t impact this real-time performance. Indeed, the first decoding step needs to be performed after collecting a representative number of trials (typically, 60 for 4 attention positions). The second decoding step can be performed directly after this first step. These two steps are very easily performed during an inter-trial interval that typically lasts for 200 to 500 ms. In other words, the proposed two-step decoding enhances the attention decoding accuracy, with no impact on the real-time performance of the decoder.

Overall, our work presents two major advances in the field of real-time access to the attentional spotlight locus. First we demonstrate that this spotlight location can be estimated from both MUA and LFP signals. Second, we introduce a novel two-step decoding method that further enhances the behavioral relevance of the decoded attentional spotlight. Most crucially, our work illustrates the tremendous benefit of adapting machine learning strategies to the specific functional properties of the cognitive function under study.

Data & code availability

All data and code used in this study are available via a request to the corresponding author after signing the data and code sharing agreement approved by the Centre National pour la Recherche Scientifique (CNRS). This data/code sharing procedures are in line with the requirements of the funding agencies.

Contributions

Conceptualization, S.B.H. C.D.F. and C.G.; Data Acquisition, S.B.H.H., F.D.B.; Methodology, C.D.F. C.G and S.B.H.; Investigation, C.D.F. C.G and S.B.H; Writing – Original Draft C.D.F. C.G and S.B.H; Writing – Review & Editing, C.D.F. C.G and S.B.H; Funding Acquisition, S.B.H.; Supervision, S.B.H.

Acknowledgments

S.B.H was supported by ERC Brain3.0 #681978, ANR-11-BSV4-0011 & ANR-14-ASTR-0011-01, LABEX CORTEX funding (ANR-11-LABX-0042) from the Université de Lyon, within the program Investissements d’Avenir (ANR-11-IDEX-0007) operated by the French National Research Agency (ANR). C.D.S.F. and C.G. were supported by ERC Brain3.0 #681978. We thank research engineer Serge Pinède for technical support and Jean-Luc Charieau and Fidji Francioly for animal care. All procedures were approved by the local animal care committee (C2EA42-13-02-0401-01) and the Ministry of research, in compliance with the European Community Council, Directive 2010/63/UE on Animal Care.

Supplementary materials

Supplementary material associated with this article can be found, in the online version, at doi:10.1016/j.neuroimage.2021.117853.

References

Andersen, R. A., Hwang, E. J., Mulliken, G. H., 2010. Cognitive Neural Prosthetics. Annu. Rev. Psychol. 61, 169–C3. doi:10.1146/annurev.psych.093008.100503.

Andersson, P., Pluim, J.P.W., Siero, J.C.W., Klein, S., Viergever, M.A., Ramsey, N.F., 2011. Real-time decoding of brain responses to visuospatial attention using 7T fMRI. PLoS ONE 6, e27638. doi:10.1371/journal.pone.0027638.

Andersson, P., Ramsey, N.F., Raemaekers, M., Viergever, M.A., Pluim, J.P.W., 2012. Real-time decoding of the direction of covert visuospatial attention. J. Neural. Eng. 9, 045004. doi:10.1088/1741-2560/9/4/045004.

Astrand, E., Enel, P., Ibos, G., Dominey, P.F., Baraduc, P., Hamed, S.B., 2014a. Comparison of classifiers for decoding sensory and cognitive information from prefrontal neuronal populations. PLoS ONE 9, e86314. doi:10.1371/journal.pone.0086314.

Astrand, E., Ibos, G., Duhamel, J.-.R., Ben Hamed, S., 2015. Differential dynamics of spatial attention, position, and color coding within the parietofrontal network. J. Neurosci. 35, 3174–3189. doi:10.1523/JNEUROSCI.2370-14.2015.

Astrand, E., Wardak, C., Baraduc, P., Ben Hamed, S., 2016. Direct two-dimensional access to the spatial location of covert attention in macaque prefrontal cortex. Curr. Biol. 26, 1699–1704. doi:10.1016/j.cub.2016.04.054.

Astrand, E., Wardak, C., Ben Hamed, S., 2020. Neuronal population correlates of target selection and distractor filtering. Neuroimage 209, 116517. doi:10.1016/j.neuroimage.2020.116517.

Astrand, E., Wardak, C., Ben Hamed, S., 2014b. Selective visual attention to drive cognitive brain–machine interfaces: from concepts to neurofeedback and rehabilitation applications. Front. Syst. Neurosci. 8. doi:10.3389/fnsys.2014.00144.

Bae, G.-Y., Luck, S.J., 2018. Dissociable Decoding of Spatial Attention and Working Memory from EEG Oscillations and Sustained Potentials. J. Neurosci 38, 409–422. doi:10.1523/JNEUROSCI.2860-17.2017.

Bruce, C.J., Goldberg, M.E., 1985. Primate frontal eye fields. I. Single neurons discharging before saccades. J. Neurophysiol. 53, 603–635. doi:10.1152/jn.1985.53.3.603.

Bruce, C.J., Goldberg, M.E., Bushnell, M.C., Stanton, G.B., 1985. Primate frontal eye fields. II. Physiological and anatomical correlates of electrically evoked eye movements. J. Neurophysiol. 54, 714–734. doi:10.1152/jn.1985.54.3.714.

Buschman, T.J., Miller, E.K., 2007. Top-down versus bottom-up control of attention in the prefrontal and posterior parietal cortices. Science 315, 1860–1862. doi:10.1126/science.1138071.

Chalk, M., Herrero, J.L., Gieselmann, M.A., Delicato, L.S., Gotthardt, S., Thiele, A., 2010. Attention reduces stimulus-driven gamma frequency oscillations and spike field Coherence in V1. Neuron 66, 114–125. doi:10.1016/j.neuron.2010.03.013.

Cinel, C., Valeriani, D., Poli, R., 2019. Neurotechnologies for Human Cognitive Augmentation: Current State of the Art and Future Prospects. Front. Hum. Neurosci. 13. doi:10.3389/fnhum.2019.00013.

Desantis, A., Chan-Hon-Tong, A., Collins, T., Hogendoorn, H., Cavanagh, P., 2020. Decoding the temporal dynamics of covert spatial attention using multivariate EEG analysis: contributions of raw amplitude and alpha power. Front. Hum. Neurosci. 14. doi:10.3389/fnhum.2020.570419.

Di Bello, F., Ben Hadj Hassen, S., Astrand, E., Ben Hamed, S., 2020. Selection and suppression of visual information in the macaque prefrontal cortex. bioRxiv doi:10.1101/2020.03.25.007922.

Dresler, M., Sandberg, A., Bublitz, C., Ohla, K., Trenado, C., Mroczko-Wąsowicz, A., Kühn, S., Repantis, D., 2018. Hacking the Brain: Dimensions of Cognitive Enhancement. Neurosci. 10, 1137–1148. doi:10.1021/acschemneuro.8b00571.

Ekstrom, L.B., Roelfsema, P.R., Arsenault, J.T., Bonmassar, G., Vanduffel, W., 2008. Bottom-up dependent gating of frontal signals in early visual cortex. Science 321, 414–417. doi:10.1126/science.1153276.

Enriquez-Geppert, S., Huster, R.J., Herrmann, C.S., 2017. EEG-Neurofeedback as a Tool to Modulate Cognition and Behavior: A Review Tutorial. Front. Hum. Neurosci. 11. doi:10.3389/fnhum.2017.00051.

Farbod Kia, S., Astrand, E., Ibos, G., Ben Hamed, S., 2011. Readout of the intrinsic and extrinsic properties of a stimulus from un-experienced neuronal activities: towards cognitive neuroprostheses. J. Physiol. Paris 105, 115–122. doi:10.1016/j.jphysparis.2011.07.015.

Fiebelkorn, I.C., Pinsk, M.A., Kastner, S., 2018. A dynamic interplay within the frontoparietal network underlies rhythmic spatial attention. Neuron 99, 842–853.e8. doi:10.1016/j.neuron.2018.07.038.

Fries, P., 2015. Rhythms for cognition: communication through coherence. Neuron 88, 220–235. doi:10.1016/j.neuron.2015.09.034.

Fries, P., Reynolds, J.H., Rorie, A.E., Desimone, R., 2001. Modulation of oscillatory neuronal synchronization by selective visual attention. Science 291, 1560–1563. doi:10.1126/science.1055465.

Gaillard, C., Ben Hadj Hassen, S., Di Bello, F., Bihan-Poudec, Y., VanRullen, R., Ben Hamed, S., 2020. Prefrontal attentional saccades explore space rhythmically. Nat. Commun. 11, 925. doi:10.1038/s41467-020-14649-7.

Ghadikolaei, H.S., Ghauch, H., Fischione, C., Skoglund, M., 2019. Learning and data selection in big datasets. In: International Conference on Machine Learning. Presented at the International Conference on Machine Learning, PMLR, pp. 2191–2200.

Gregoriou, G.G., Gotts, S.J., Zhou, H., Desimone, R., 2009. High-frequency, long-range coupling between prefrontal and visual cortex during attention. Science 324, 1207–1210. doi:10.1126/science.1171402.

Gunduz, A., Brunner, P., Daitch, A., Leuthardt, E.C., Ritaccio, A.L., Pesaran, B., Schalk, G., 2012. Decoding covert spatial attention using electrocorticographic (ECoG) signals in humans. Neuroimage 60, 2285–2293. doi:10.1016/j.neuroimage.2012.02.017.

Hubbard, J., Kikumoto, A., Mayr, U., 2019. EEG decoding reveals the strength and temporal dynamics of goal-relevant representations. Sci. Rep. 9, 9051. doi:10.1038/s41598-019-45333-6.

Ibos, G., Duhamel, J.-.R., Ben Hamed, S., 2013. A functional hierarchy within the parietofrontal network in stimulus selection and attention control. J. Neurosci. 33, 8359–8369. doi:10.1523/JNEUROSCI.4058-12.2013.

Jiang, Y., Abiri, R., Zhao, X., 2017. Tuning Up the Old Brain with New Tricks: Attention Training via Neurofeedback. Front. Aging Neurosci. 9. doi:10.3389/fnagi.2017.00052.

Kerkoerle, T.van, Self, M.W., Dagnino, B., Gariel-Mathis, M.-.A., Poort, J., Togt, C., van der, Roelfsema, P.R., 2014. Alpha and gamma oscillations characterize feedback and feedforward processing in monkey visual cortex. PNAS 111, 14332–14341. doi:10.1073/pnas.1402773111.

Kienitz, R., Schmiedt, J.T., Shapcott, K.A., Kouroupaki, K., Saunders, R.C., Schmid, M.C., 2018. Theta rhythmic neuronal activity and reaction times arising from cortical receptive field interactions during distributed attention. Curr. Biol. 28. doi:10.1016/j.cub.2018.05.086, undefined-undefined.

Kitamura, G., Deible, C., 2020. Retraining an open-source pneumothorax detecting machine learning algorithm for improved performance to medical images. Clin. Imaging 61, 15–19. doi:10.1016/j.clinimag.2020.01.008.

Leszczyński, M., Barczak, A., Kajikawa, Y., Ulbert, I., Falchier, A.Y., Tal, I., Haegens, S., Melloni, L., Knight, R.T., Schroeder, C.E., 2020. Dissociation of broadband high-frequency activity and neuronal firing in the neocortex. Sci. Adv. 6, eabb0977. doi:10.1126/sciadv.abb0977.

Moore, T., Fallah, M., 2001. Control of eye movements and spatial attention.. Proc Natl Acad Sci USA 98 (3), 1273–1276. doi:10.1073/pnas.021549498.

Morioka, H., Kanemura, A., Morimoto, S., Yoshioka, T., Oba, S., Kawanabe, M., Ishii, S., 2014. Decoding spatial attention by using cortical currents estimated from electroencephalography with near-infrared spectroscopy prior information. Neuroimage 90, 128–139. doi:10.1016/j.neuroimage.2013.12.035.

Nandy, A.S., Nassi, J.J., Reynolds, J.H., 2017. Laminar organization of attentional modulation in macaque visual area V4. Neuron 93, 235–246. doi:10.1016/j.neuron.2016.11.029.

Niu, X., Yang, K., Zhang, G., Yang, Z., Hu, X., 2020. A pretraining-retraining strategy of deep learning improves cell-specific enhancer predictions. Front. Genet. 10. doi:10.3389/fgene.2019.01305.

Oostenveld, R., Fries, P., Maris, E., Schoffelen, J.-.M., 2011. FieldTrip: open source software for advanced analysis of MEG, EEG, and invasive electrophysiological data. Comput. Intell. Neurosci. 2011, 156869. doi:10.1155/2011/156869.

Ordikhani-Seyedlar, M., Lebedev, M.A., Sorensen, H.B.D., Puthusserypady, S., 2016. Neurofeedback Therapy for Enhancing Visual Attention: State-of-the-Art and Challenges. Front Neurosci 10. doi:10.3389/fnins.2016.00352.

O'Sullivan, J.A., Power, A.J., Mesgarani, N., Rajaram, S., Foxe, J.J., Shinn-Cunningham, B.G., Slaney, M., Shamma, S.A., Lalor, E.C., 2015. Attentional selection in a cocktail party environment can be decoded from single-trial EEG. Cereb. Cortex 25, 1697–1706. doi:10.1093/cercor/bht355.

Paneri, S., Gregoriou, G.G., 2017. Top-down control of visual attention by the prefrontal cortex. functional specialization and long-range interactions. Front. Neurosci. 11. doi:10.3389/fnins.2017.00545.

Prochazka, A., 2017. Neurophysiology and neural engineering: a review. J. Neurophysiol. 118, 1292–1309. doi:10.1152/jn.00149.2017.

Ray, S., Crone, N.E., Niebur, E., Franaszczuk, P.J., Hsiao, S.S., 2008. Neural correlates of high-gamma oscillations (60–200 Hz) in macaque local field potentials and their potential implications in electrocorticography. J. Neurosci. 28, 11526–11536. doi:10.1523/JNEUROSCI.2848-08.2008.

Richter, C.G., Thompson, W.H., Bosman, C.A., Fries, P., 2017. Top-down beta enhances bottom-up gamma. J. Neurosci. 37, 6698–6711. doi:10.1523/JNEUROSCI.3771-16.2017.

Rotermund, D., Ernst, U.A., Mandon, S., Taylor, K., Smiyukha, Y., Kreiter, A.K., Pawelzik, K.R., 2013. Toward high performance, weakly invasive brain computer interfaces using selective visual attention. J. Neurosci. 33, 6001–6011. doi:10.1523/JNEUROSCI.4225-12.2013.

Saalmann, Y.B., Pinsk, M.A., Wang, L., Li, X., Kastner, S., 2012. Pulvinar regulates information transmission between cortical areas based on attention demands. Science 337, 753–756. doi:10.1126/science.1223082.

Salari, N., Büchel, C., Rose, M., 2014. Neurofeedback training of gamma band oscillations improves perceptual processing. Exp. Brain Res. 232, 3353–3361. doi:10.1007/s00221-014-4023-9.

Samaha, J., Sprague, T.C., Postle, B.R., 2016. Decoding and reconstructing the focus of spatial attention from the topography of alpha-band oscillations. J. Cogn. Neurosci. 28, 1090–1097. doi:10.1162/jocn_a_00955.

Thiery, T., Lajnef, T., Jerbi, K., Arguin, M., Aubin, M., Jolicoeur, P., 2016. Decoding the Locus of Covert Visuospatial Attention from EEG Signals. PLoS ONE 11 (e0160304). doi:10.1371/journal.pone.0160304.

Treder, M.S., Bahramisharif, A., Schmidt, N.M., van Gerven, M.A., Blankertz, B., 2011. Brain-computer interfacing using modulations of alpha activity induced by covert shifts of attention. J. Neuroeng. Rehabil. 8, 24. doi:10.1186/1743-0003-8-24.

Tremblay, S., Doucet, G., Pieper, F., Sachs, A., Martinez-Trujillo, J., 2015. Single-trial decoding of visual attention from local field potentials in the primate lateral prefrontal cortex is frequency-dependent. J. Neurosci. 35, 9038–9049. doi:10.1523/JNEUROSCI.1041-15.2015.

van Gerven, M., Jensen, O., 2009. Attention modulations of posterior alpha as a control signal for two-dimensional brain–computer interfaces. J. Neurosci. Method. 179, 78–84. doi:10.1016/j.jneumeth.2009.01.016.

Wardak, C., Ibos, G., Duhamel, J.-.R., Olivier, E., 2006. Contribution of the monkey frontal eye field to covert visual attention. J. Neurosci. 26, 4228–4235. doi:10.1523/JNEUROSCI.3336-05.2006.

Zhang, Y., Meyers, E.M., Bichot, N.P., Serre, T., Poggio, T.A., Desimone, R., 2011. Object decoding with attention in inferior temporal cortex. PNAS 108, 8850–8855. doi:10.1073/pnas.1100999108.